Letter | Editors' Suggestion | Featured in Physics

Pinned adcolloids disfavor nucleation in colloidal vapor deposition

Noman Hanif Barbhuiya,[1] Pritam K. Mohanty,[1] Saikat Mondal,[2] Aminul Hussain,[1] Adhip Agarwala,[2] and Chandan K. Mishra[1,*]

[1]*Department of Physics, Indian Institute of Technology Gandhinagar, Palaj, Gandhinagar 382055, Gujarat, India*

[2]*Department of Physics, Indian Institute of Technology Kanpur, Kalyanpur, Kanpur 208016, Uttar Pradesh, India*

(Received 16 January 2025; accepted 10 April 2025; published 30 May 2025)

Crystallization through vapor deposition is ubiquitous and is inevitably influenced by impurities that often impact the local structure. Interestingly, the effect of immobilizing some of the depositing particles themselves, which would preserve local structural symmetry, remains largely unexplored. Herein, we perform colloidal vapor deposition on a substrate with a few pinned adcolloids, termed "mobility impurities." Through thermodynamic and kinematic measurements, we demonstrate that these pinned adcolloids, even though they share identical geometry and interaction with depositing particles, are disfavored as nucleation centers. Our experimental findings, supported by molecular dynamics simulations and a simple theoretical model, reveal that entropic contributions, rather than energetic ones, govern nucleation physics in the presence of mobility impurities. Moreover, tuning the mobility of colloids on the substrate adjusts the nucleation likelihood at pinned sites. In later stages of growth, pinning induces mode localization and alters the thin film's vibrational spectrum. Our work thus underscores the potential of strategically incorporating mobility impurities to engineer material properties.

DOI: 10.1103/PhysRevE.111.L053403

The introduction of impurities, whether intentional or otherwise, during the initial stages of material fabrication holds considerable sway over a spectrum of material properties and their ensuing performance, such as structure [1,2], mechanical strength [3,4], and transport properties [5,6]. These impurities, often extrinsic, differ from the primary constituents of the material in terms of one or more physical and chemical attributes, and exert their influence by modifying the free energy landscape, thereby altering nucleation and growth mechanisms of the materials [7–11]. For example, in processes akin to vapor deposition, the presence of impurities can lead to diverse outcomes: they might lower the interfacial barriers to crystallization [7] and promote smoother film formation with reduced defect density [12,13], regulate the rate of nucleation and the morphology of growing islands [1], or impede crystal growth altogether [10,14]. However, a high density of immobile impurities on the substrate frustrates crystal nucleation [15] and would lead to a structurally disordered phase.

A thorough understanding of the precise influence of impurities requires disentangling multiple complex processes at play during these early stages of material fabrication. These include the shape and height of the diffusion barrier of impurities on the substrate relative to the primary constituents [7,10,11,16], as well as the nature of their interactions with the primary constituents compared with the interactions between the primary constituents themselves [2,7,17]. Importantly, these factors encompass both thermodynamic and kinematic aspects. For instance, the relative interaction strengths and entropy dictate the thermodynamic favorability of certain configurations [18] while diffusion barriers govern the kinematics of particle movement and rearrangement [16]. A clear microscopic understanding, therefore, requires a systematic and controlled isolation of these factors to elucidate their individual impacts. Interestingly, colloidal vapor deposition offers an excellent experimental platform to systematically isolate and elucidate the role of each of these factors arising due to the presence of impurities on the physics of nucleation processes, wherein their influence is most prominent [19,20].

Here, we uncover the role of contrasting diffusion barriers of impurities and the primary constituents (adcolloids) on the substrate in colloidal vapor deposition while keeping all other attributes between them identical. To achieve this, we randomly immobilize (pin) a tiny fraction of depositing colloids themselves on the substrate prior to starting the deposition experiments. These pinned particles would share the same interaction potential with the depositing colloids, but differ in their lack of mobility, and thus we term them "mobility impurities" [21]. Henceforth, "mobility impurities" and "pinned particles" will be used interchangeably in this Letter to refer to pinned adcolloids.

We employ video microscopy to observe the spatiotemporal evolution of clusters, encompassing their formation, disintegration, and growth at a single-particle level, both with and without pinned particles (Supplemental Movies S1 and S2) [22,23]. By developing novel analytical tools to understand the experimental data, we find distinct thermodynamic and kinematic mechanisms governing the colloid aggregation based on the presence or absence of pinned adcolloids in precursor clusters. Supported by minimal theoretical models and molecular dynamics simulations, our experiments reveal

*Contact author: chandan.mishra@iitgn.ac.in

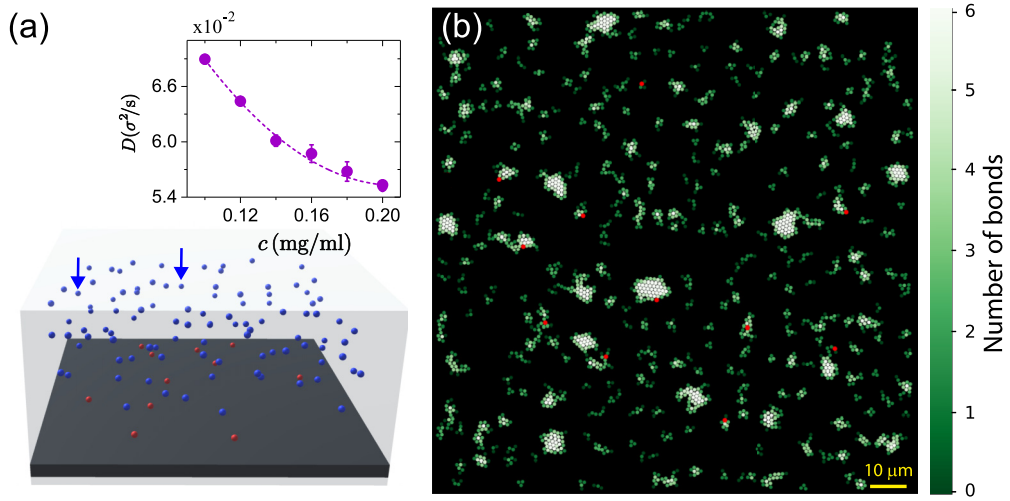

FIG. 1. Experimental setup and characterization. (a) Schematic of the experimental setup showing pinned colloidal particles in red and sedimenting ones in blue. Inset shows the surface diffusivity of single colloids, D (in the units of σ^2/s), versus c. The dashed curve is a guide for the eye. Error bars for $0.12 \leqslant c \leqslant 0.18$ mg/ml represent the standard error of the mean from two independent experiments. For $c = 0.20$ mg/ml, the error bars correspond to the fitting error. (b) Snapshot of the field-of-view at monolayer coverage, $\Theta \sim 0.17$, at $c = 0.12$ mg/ml. The particles have been color-coded based on the number of bonds they form in their nearest-neighbor shell. Pinned particles are shown in red.

that pinning decreases the entropic contributions to the free energy, rendering pinned sites *disfavorable* for nucleation (Supplemental Movie S3) [22]. Moreover, the entropic constraint grows as the mobility of the depositing colloids on the substrate decreases, providing a mechanism to control nucleation propensity at pinned sites. Thus, our work provides direct evidence that the physics of nucleation in the presence of these mobility impurities in colloidal vapor deposition is primarily entropy-driven, rather than driven by energetic considerations.

Figure 1(a) schematically illustrates our experimental setup for vapor deposition. Silica colloidal particles of diameter $\sigma \sim 1.0$ μm were allowed to sediment onto a glass substrate under gravity at a steady flux of $F = (5.1 \pm 0.1) \times 10^{-5}$ monolayers/s (Supplemental Note S1) [22,24,25]. The sedimenting colloids, upon reaching the substrate, diffuse on the surface with diffusivity, $D \sim 6 \times 10^{-2}\sigma^2/s$ [inset of Fig. 1(a), Supplemental Note S2, Supplemental Movies S1 and S2] [22]. Thus, the sole control parameter in vapor deposition experiments, D/F, approaches the practically achievable upper limit in colloidal deposition experiments, which in our case turns out to be $D/F \sim 10^3$ [26]. Prior to the start of the experiment, the glass substrate was featured with randomly positioned pinned particles that matched the sedimenting colloids in shape, size, and interparticle interactions but differed only in mobility. In all experiments, the pinned sites are sparsely distributed, with an average nearest-neighbor distance between pinned particles, $L_p \sim 22\sigma$, with a minimum separation of 10σ between them. This ensures that nucleation events at one pinned site are independent of others (Supplemental Note S1) [22]. Moreover, since L_p was significantly larger than the mean diffusion length, $l \sim 5 - 6\sigma$, of the depositing colloids on the substrate, nucleation events, whether involving pinned particles or not, were not only independent but occurred under identical experimental conditions.

The depositing colloids, after sedimentation, eventually aggregate with neighboring colloids, either with or without a pinned particle. To minimize the desorption of sedimented colloids from the substrate, nonadsorbing depletants were added to the colloidal suspension, inducing short-range attractive forces between colloids and the substrate and between colloids themselves. The introduction of depletants serves another purpose in our experiments: increasing the concentration of depletant particles, c, decreases the diffusivity of colloids on the substrate [inset of Fig. 1(a)]. A reduction in D decreases mobility contrast between the pinned and free adcolloids, and thus, c could be a control parameter for modulating the probability of nucleation at pinned sites. Strikingly, regardless of the value of c, pinned sites were seldom observed at the center of the growing precursor clusters [Fig. 1(b) and Supplemental Fig. S2] [22], indicating that thermodynamics and kinematics of the nucleation mechanism may be altered in the presence of mobility impurities. To this end, we developed novel analytic tools to directly measure these relevant parameters utilizing particle trajectories extracted from our video microscopy experiments.

For cluster nucleation to be favored at the pinned sites, the free energy difference between precursor clusters of a specific size n, comprising a pinned particle and those composed of only free particles, must be negative, that is, $\Delta F_{p-f}(n) = [\Delta U_{p-f}(n) - T\,\Delta S_{p-f}(n)] < 0$. Here, $\Delta U_{p-f}(n)$ and $\Delta S_{p-f}(n)$ are the differences in the internal energy and entropy between clusters of the same size n formed with a pinned particle and without it, and T is the temperature. In our calculations utilizing experimental data, $\Delta U_{p-f}(n)$ and $\Delta S_{p-f}(n)$ are ensemble averaged over all the clusters of size n appearing over the total experimental duration, $t_{\mathrm{tot}} \sim 10^4$ s. However, note that primary contributions to the statistics arise predominantly from the early stages of film growth (Supplemental Fig. S3) [22].

Given the steady low flux rate ($\sim 10^{-5}$ monolayers/s) and typical diffusivity of about $10^{-2}\sigma^2/\mathrm{s}$, the nucleation processes at individual precursor clusters can be considered in a quasistatic equilibrium with the local environment (Supple-

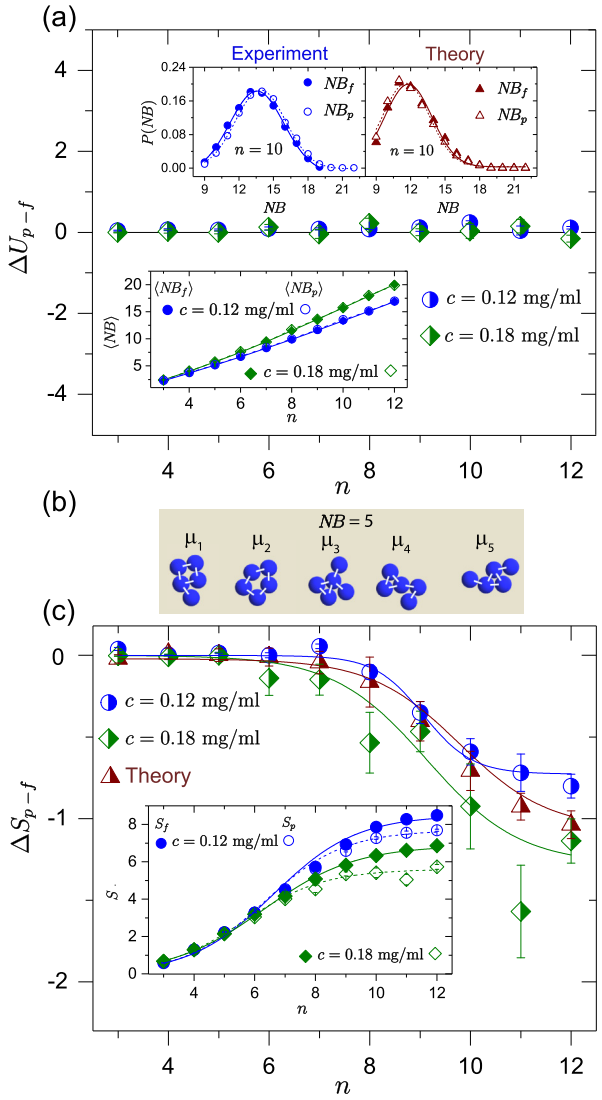

FIG. 2. Internal energy and entropy of precursor clusters. (a) $\Delta U_{p-f}(n)$ in the units of scaled k_BT versus n at different c. The top panel inset shows $P(NB)$ for $n = 10$ − particle clusters from the experiment at $c = 0.12$ mg/ml (left) and theory (right). The bottom inset shows $\langle NB(n) \rangle$ versus n. Open and closed symbols represent data for clusters with and without a pinned particle, respectively. (b) Enumeration of experimentally observed topologically distinct coarse-grained microstates, $\{\mu_i\}$, for $n = 5$ and $NB = 5$, with unique arrangements of bond connectivity. (c) $\Delta S_{p-f}(n)$ in the units of k_B versus n for the same c as in (a) and theoretical model (brown triangles). The inset shows the entropy of clusters as a function of n. Open and closed symbols represent data for clusters with and without a pinned particle, respectively. For theoretical curves in (a) and (c), cluster distributions are obtained from steady-state configurations of a Markov matrix governing hard spheres hopping on a triangular lattice of 256 sites. About 10^5 configurations are taken for each of the particle densities between 0.1 and 0.6 in intervals of 0.01, and for the pinning case, 1% of sites are kept immobilized. Solid and dashed curves in (a) and (c) are guides for the eye. Error bars in data points represent the standard error of the mean from two different experiments at the same c, consisting of $\sim 10^4 - 10^5$ data points.

mental Note S3) [22]. Hence, we employed and measured conventional thermodynamic variables such as $\Delta U_{p-f}(n)$ and $\Delta S_{p-f}(n)$ from the observations of the colloid dynamics to investigate any potential preferential nucleation at pinned sites.

Due to the short-range nature of depletion-induced attraction, the internal energy of a cluster with a fixed size n is proportional to the number of bonds, $NB(n)$, in the cluster [18]. Analyzing all the cluster configurations appearing over t_{tot}, we find the probability distribution of finding NB bonds for a given cluster size, $P(NB)$, to be unimodal for all n, irrespective of whether a cluster contains a pinned particle or not [top left inset of Fig. 2(a)].

Next, using $P(NB)$, we find the average number of bonds, $\langle NB(n) \rangle$, for each n [bottom inset of Fig. 2(a)], and subsequently estimate $\Delta U_{p-f}(n)$ [Fig. 2(a)]. As expected, for a fixed c, $\langle NB(n) \rangle$ increases with n. For a given n, $\langle NB(n) \rangle$ increases with c due to increased interparticle attraction favoring compact cluster configurations. Interestingly, $\langle NB(n) \rangle$ exhibits similar trends for clusters with and without a pinned particle, yielding $\Delta U_{p-f}(n) \sim 0$ [Fig. 2(a)]. Thus, from the perspective of internal energy, the inclusion of a pinned particle in precursor clusters may have no impact on their thermodynamic stability. Having discussed the role of internal energy, we shift our focus to entropic contributions to free energy.

When considering a cluster of size n, multiple unique bond connectivities are possible for a fixed NB, which we define as topologically distinct coarse-grained microstates, $\{\mu_i\}$ [Fig. 2(b)] [27]. Thus, we can determine the entropic contributions by the identification and enumeration of these microstates. To catalog the unique microstates, we map all bond configurations for each n onto their respective adjacency matrices, $A_{n\times n}$. Each element $a_{(l,m)}$ of this matrix indicates the presence (1) or absence (0) of a bond between particles l and m. Subsequently, we identify the unique isomorphic bond configurations (microstates) [28–30] and obtain the probabilities $p(\mu_i)$ for each μ_i corresponding to a particular n (Supplemental Note S4 and Supplemental Fig. S4) [22]. The entropy of a cluster of size n can then be defined as $S(n) = -k_B \sum_i [p(\mu_i) \log(p(\mu_i))]_n$ (Supplemental Note S5) [22]. Here, $p(\mu_i)$ represents the probability of the i^{th} unique microstate and k_B is the Boltzmann constant. Unlike internal energy, the entropy for $n \geqslant 7$ exhibits a distinct profile between clusters featuring a pinned particle and those comprising only free particles [inset of Fig. 2(c)]. For a given c, $\Delta S_{p-f} < 0$ [Fig. 2 (c)], leading to $\Delta F_{p-f} > 0$, suggesting that pinned particles are disfavorable for nucleation.

For a cluster of size n containing a pinned particle, the number of free particles is $n - 1$. As n increases, both the number of free particles in the cluster and the total degrees of freedom increase, while the restricted degrees of freedom due to pinning remain constant. Therefore, one would expect the impact of a pinned particle to diminish as n grows. However, our experiments suggest otherwise, indicating that pinning *even a single particle* in precursor clusters significantly impacts its nucleation mechanism and the free energy landscape. Moreover, as evidenced by the variation of ΔS_{p-f} with c, the

entropic constraints on clusters with a pinned particle increase with decreasing D [Fig. 2(c)]. Thus, c can be adjusted to tune nucleation likelihood at pinned sites.

Guided by experimental phenomenology, we construct a minimal theoretical model. Modeling colloids as hard spheres hopping on a triangular lattice, the Markov matrix can be mapped to a ferromagnetic spin$-1/2$ Heisenberg model [31,32]. The ground state of such a Hamiltonian, corresponding to the steady state of the Markov matrix, represents an equal probability distribution of all possible states of a fixed number of particles on the lattice, satisfying the hard sphere constraint. Pinning a particle thus corresponds to fixing a spin to $+1/2$ state on the particular site in the Heisenberg lattice Hamiltonian (Supplemental Note S6) [22].

By sampling typical configurations in the steady state ($\sim 10^5$), we isolate the cluster distributions for a fixed cluster size n, both with and without a pinned particle (Supplemental Note S6) [22]. Consistent with the experimental findings, we observe no significant change in $P(NB)$ due to pinning of a particle [top right inset to Fig. 2(a) and Supplemental Figs. S5 and S6] [22]. This indicates that the bond probability distribution is primarily governed by lattice animal configurations rather than energetic considerations [33–35]. Furthermore, the configurational entropy of the clusters reveals that pinning a particle indeed reduces the entropy of the cluster [Fig. 2(c) and Supplemental Fig. S7] [22], making them less favorable for nucleation. This also makes it plausible why pinned sites either remain single entities or are predominantly located at the edge of the crystallite in our experiments [Fig. 1(b) and Supplemental Fig. S2] [22].

Interestingly, since we consistently observe that $\Delta F_{p-f} \sim 0$ for $n < 7$ in our experiments and theoretical model, it is crucial to determine whether the impact of mobility impurities in nucleation mechanisms diminishes with increasing c. At higher c, nucleation is expected to initiate at smaller cluster sizes compared with those at smaller c. Hence, we first attempt to identify the critical nuclei size, n_c, at all c studied in this work, and for both scenarios, with and without pinned particles. n_c marks the threshold where cluster growth becomes favorable (Supplemental Fig. S8) [22]. To determine n_c, we track all clusters of size n, starting with $n = 2$, with time and their subsequent most probable cluster size. For a given c, n_c is defined as the smallest n for which the subsequent most probable cluster size exceeds n. In addition, for all $n \geqslant n_c$, the next most probable cluster size must be greater than n.

We find that, for clusters formed of all free particles, n_c can be determined for all c and are within the range $4 \leqslant n_c \leqslant 13$ (Supplemental Fig. S9) [22]. However, surprisingly, with a pinned particle, the analysis for n_c displays no discernible trend at any c (Supplemental Fig. S8) [22], indicating a significant disruption to the nucleation process of precursor clusters. The disruption in the nucleation process for clusters containing a pinned particle can be understood using thermodynamic arguments for clusters of size $n \geqslant 7$ (Fig. 2), which is the case for $c \leqslant 0.14$ mg/ml, where $n_c > 7$ (Supplemental Fig. S9) [22].

However, as c increases, n_c decreases, leading to a regime where $n_c < 7$, and the free energy difference is negligible ($\Delta F_{p-f} \sim 0$) between clusters with and without a pinned particle. In other words, the thermodynamic analyses suggest that clusters of size $n < 7$, regardless of whether they contain a pinned particle or not, can access similar energy states with similar probabilities. However, the persistent difficulty in determining n_c for clusters with a pinned particle for $c \geqslant 0.16$ mg/ml implies that the equilibrium thermodynamic approach is insufficient to explain the observed nucleation mechanism. We, therefore, turn to investigate the rate at which individual clusters transition between configurations and if pinning causes any geometrical obstructions or "kinematic bottlenecks" in the configurational landscape of clusters containing a pinned particle [36].

During the initial stages of vapor deposition, colloids from the bulk join the precursor clusters on the substrate. The rate at which these clusters navigate their energy landscape dictates the fate of precursor clusters and sets the stage for the stability and growth of larger clusters (and crystallites). For instance, in vapor-deposited molecular glasses, faster surface diffusion of molecules enhances their stability [37,38]. Similarly, here, identically sized clusters having equivalent thermodynamic stability may still differ kinematically, influencing their suitability for ensuing growth. The rearrangement of particles within each cluster leads to the exploration of various microstates. Consequently, the rate of exploration dictates the pace of navigating the free energy landscape, while the number of unique particles involved ensures thoroughness in this exploration.

To quantify the rate, we track the temporal evolution of all clusters of size n as they transition between different microstates, μ_k, at a fixed time interval [Fig. 3(a)]. For a cluster surviving for a time t_k with cumulative instances of transitions C_k, we quantify the rate of accessing microstates $\dot{\mu}(n) = \left[\langle \frac{C_k}{t_k} \rangle_k\right]_n$, where $\langle\cdot\rangle_k$ represents ensemble average over all the clusters, k, of size n. Similarly, the rate associated with the total number of unique particles, $\mathcal{N}_k$, that participate in μ_k over t_k is $\dot{\mathcal{N}}(n) = \left[\langle \frac{\mathcal{N}_k}{t_k} \rangle_k\right]_n$. Note that the necessity for clusters to persist sufficiently longer in time precludes any such analysis for $n > 7$, the range already explored through thermodynamic arguments.

As anticipated, for a fixed c, both $\dot{\mu}(n)$ and $\dot{\mathcal{N}}(n)$ increase with n [Figs. 3(c) and 3(d) and Supplemental Fig. S10] [22]. Remarkably, while $\Delta F_{p-f} \sim 0$ for $n < 7$, $\dot{\mu}(n)$ and $\dot{\mathcal{N}}(n)$ are consistently lower for clusters containing a pinned particle [Figs. 3(c) and 3(d)] and Supplemental Fig. S10] [22]. Thus, pinning a particle in clusters not only slows its traversal through the free energy landscape but also engages fewer unique particles in their exploration. This hampers the ability of clusters with a pinned particle to promptly attain a stable configuration, as evidenced by the difficulty in determining n_c (Supplemental Fig. S8) [22]. Taken together, for small precursor clusters ($n < 7$) exhibiting identical thermodynamic stability irrespective of the presence or absence of a pinned particle in them, the kinematic constraints arising due to pinning are the primary impediment to nucleation at the pinned sites. Beyond $n \geqslant 7$, while kinematic restrictions should persist, the thermodynamic penalty associated with reduced configurational entropy also

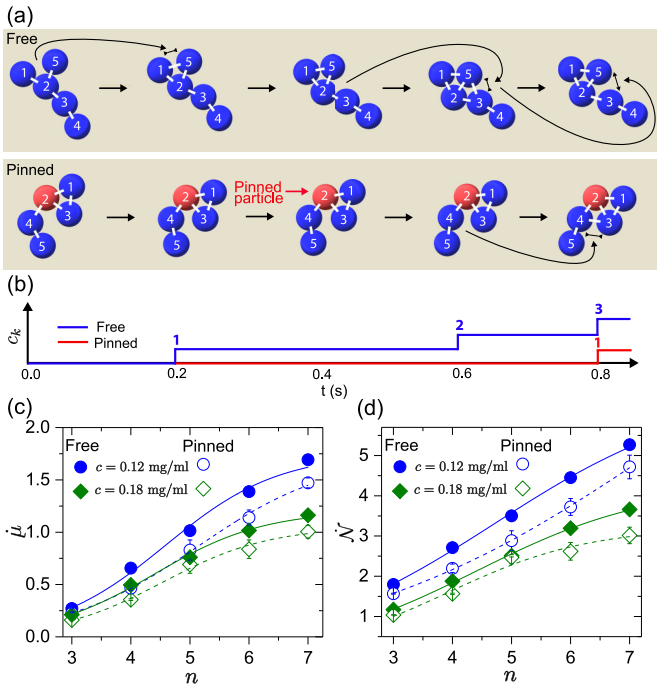

FIG. 3. Kinematics of precursor clusters. (a) Rendering from the experiment at $c = 0.12$ mg/ml to illustrate the change in microstate for a given $5-$particle cluster comprising all free particles (top) and with one pinned particle (bottom) at $\Delta t = 0.2$ s. (b) Counter, c_k, tracking microstate transitions in a cluster with all free particles (blue line) and with one pinned particle (red line) for the temporal evolution of clusters shown in (a). (c) $\dot{\mu}(n)$ and (d) $\dot{\mathcal{N}}(n)$ versus n for clusters (persisting for at least 0.5 s) with one pinned particle (open symbols) and with all free particles (solid symbols) at different c. Solid and dashed curves in (c) and (d) are guides for the eye. Error bars represent the standard error of the mean from two different experiments at the same c, consisting of $\sim 10^4 - 10^5$ data points.

plays a significant role in disfavoring nucleation events at pinned sites.

Our study unveils the critical influence of mobility impurities with unchanged interparticle interaction potential of pinned particles with depositing ones on nucleation and growth of precursor clusters in colloidal vapor deposition. Through a combination of thermodynamic and kinematic measurements, using both experiments and associated theoretical insights, we demonstrate that pinned adcolloids fail to serve as preferred nucleation sites. While thermodynamic arguments help understand such a trend for large cluster sizes, kinematics dictates the nucleation phenomena for small clusters. Importantly, the nucleation probability at pinned sites can be further modulated by manipulating the mobility of free colloids on the substrate. Notably, the findings from our study on nucleation mechanisms in the presence of mobility impurities, in principle, are expected to extend to other D/F values as well, provided $l < L_p$. However, the disparity in nucleation behavior at a pinned site and without it is expected to be amplified at low D/F values, where diffusive exploration is more restricted relative to the deposition rate.

While our experiments reveal the crucial role of configurational entropy in governing the nucleation mechanism in colloidal vapor deposition in the presence of mobility impurities, molecular dynamics simulations under experimental-like conditions, using Lennard-Jones and Morse potentials [39], unambiguously establish the broader applicability of our findings (Supplemental Note S7 and Supplemental Fig. S11) [22]. Moreover, in later stages of growth, even a single pinned site induces localization of vibrational modes in the thin film (large crystallite) [40,41], potentially altering its mechanical stability (Supplemental Note S8 and Supplemental Fig. S14) [22,42,43].

These findings collectively highlight the role of mobility impurities as a novel platform for influencing nucleation, growth, and material properties during the fabrication of colloidal superstructures, contributing to a broader understanding of mesoscale design principles [42,43]. Moreover, while our investigation focused on short-range attractions relevant for clustering of colloids, the insights gained may offer valuable parallels with atomic and molecular systems, given the analogous epitaxial growth laws, albeit the underlying physics differ [26]. Future studies could examine the influence of mobility impurities on the second and subsequent layers of crystal growth, as well as explore systems with long-range interactions, directional bonding, and the effects of pinning larger crystallites, which may be relevant to self-assembly in molecular systems.

Authors thank Mahesh M. Bandi, Sriram Ramaswamy, Chandan Dasgupta, John C. Crocker, Arjun G. Yodh, Anthony Dinsmore, Samudrajit Thapa, Prasanna Venkatesh B., K. Hima Nagamanasa, Anirban Sain, Pinaki Majumdar, Sankalp Nambiar, Sivasurender Chandran, and Vinay Vaibhav for useful comments and discussions. The idea for this project originated from preliminary experimental observations made by C.K.M. during his Ph.D. studies in the Ganapathy Group at JNCASR. We acknowledge Rajesh Ganapathy for his comments on this problem. We gratefully acknowledge financial support from the Department of Science and Technology (Government of India), INSPIRE fellowship IF200274 (N.H.B.), Prime Minister Research Fellowship (S.M.), IIT Kanpur Initiation Grant through IITK/PHY/2022010 (A.A.), IIT Gandhinagar through IP/IITGN/PHY/CM/2021/11 (C.K.M.) and the Start-up Research Grant of Science and Engineering Research Board of Government of India through SRG/2021/001077 (C.K.M.).

Data availability. The data that support the findings of this article are not publicly available upon publication because it is not technically feasible, and/or the cost of preparing, depositing, and hosting the data would be prohibitive within the terms of this research project. The data are available from the corresponding author upon reasonable request.

[1] L. Granasy, T. Pusztai, J. A. Warren, J. F. Douglas, T. Börzsönyi, and V. Ferreiro, Growth of 'dizzy dendrites' in a random field of foreign particles, Nat. Mater. **2**, 92 (2003).

[2] I. Muševič, M. Skarabot, U. Tkalec, M. Ravnik, and S. Zumer, Two-dimensional nematic colloidal crystals self-assembled by topological defects, Science **313**, 954 (2006).

[3] W. Zhong, Y. Cai, and D. Tomanek, Computer simulation of hydrogen embrittlement in metals, Nature (London) **362**, 435 (1993).

[4] J. R. Kermode, L. Ben-Bashat, F. Atrash, J. Cilliers, D. Sherman, and A. De Vita, Macroscopic scattering of cracks initiated at single impurity atoms, Nat. Commun. **4**, 2441 (2013).

[5] T. Delattre, C. Feuillet-Palma, L. Herrmann, P. Morfin, J.-M. Berroir, G. Fève, B. Plaçais, D. Glattli, M.-S. Choi, C. Mora *et al.*, Noisy Kondo impurities, Nat. Phys. **5**, 208 (2009).

[6] D. Mocatta, G. Cohen, J. Schattner, O. Millo, E. Rabani, and U. Banin, Heavily doped semiconductor nanocrystal quantum dots, Science **332**, 77 (2011).

[7] A. Cacciuto, S. Auer, and D. Frenkel, Onset of heterogeneous crystal nucleation in colloidal suspensions, Nature (London) **428**, 404 (2004).

[8] A. Navrotsky, Energetic clues to pathways to biomineralization: Precursors, clusters, and nanoparticles, Proc. Natl. Acad. Sci. USA **101**, 12096 (2004).

[9] S. Elhadj, J. De Yoreo, J. Hoyer, and P. Dove, Role of molecular charge and hydrophilicity in regulating the kinetics of crystal growth, Proc. Natl. Acad. Sci. USA **103**, 19237 (2006).

[10] V. W. De Villeneuve, R. P. Dullens, D. G. Aarts, E. Groeneveld, J. H. Scherff, W. K. Kegel, and H. N. Lekkerkerker, Colloidal hard-sphere crystal growth frustrated by large spherical impurities, Science **309**, 1231 (2005).

[11] E. Allahyarov, K. Sandomirski, S. U. Egelhaaf, and H. Löwen, Crystallization seeds favour crystallization only during initial growth, Nat. Commun. **6**, 7110 (2015).

[12] L. Ma, J. Zhu, W. Li, R. Huang, X. Wang, J. Guo, J.-H. Choi, Y. Lou, D. Wang, and G. Zou, Immobilized precursor particle driven growth of centimeter-sized $MoTe_2$ monolayer, J. Am. Chem. Soc. **143**, 13314 (2021).

[13] Y.-L. Hong, Z. Liu, L. Wang, T. Zhou, W. Ma, C. Xu, S. Feng, L. Chen, M.-L. Chen, D.-M. Sun *et al.*, Chemical vapor deposition of layered two-dimensional $MoSi_2N_4$ materials, Science **369**, 670 (2020).

[14] W. Ma, J. F. Lutsko, J. D. Rimer, and P. G. Vekilov, Antagonistic cooperativity between crystal growth modifiers, Nature (London) **577**, 497 (2020).

[15] H. Katsuno, K. Katsuno, and M. Sato, Effect of immobile impurities on two-dimensional nucleation, Phys. Rev. E **84**, 021605 (2011).

[16] G. L. Kellogg, Direct observation of substitutional-atom trapping on a metal surface, Phys. Rev. Lett. **72**, 1662 (1994).

[17] S. Liu, L. Bönig, J. Detch, and H. Metiu, Submonolayer growth with repulsive impurities: Island density scaling with anomalous diffusion, Phys. Rev. Lett. **74**, 4495 (1995).

[18] G. Meng, N. Arkus, M. P. Brenner, and V. N. Manoharan, The free-energy landscape of clusters of attractive hard spheres, Science **327**, 560 (2010).

[19] B. Li, D. Zhou, and Y. Han, Assembly and phase transitions of colloidal crystals, Nat. Rev. Mater. **1**, 15011 (2016).

[20] V. N. Manoharan, Colloidal matter: Packing, geometry, and entropy, Science **349**, 1253751 (2015).

[21] S. van Teeffelen, C. N. Likos, and H. Löwen, Colloidal crystal growth at externally imposed nucleation clusters, Phys. Rev. Lett. **100**, 108302 (2008).

[22] See Supplemental Material at http://link.aps.org/supplemental/10.1103/PhysRevE.111.L053403 for (i) experimental methods (ii) measurement of diffusivity of single colloids on the substrate, (iii) validity of the quasistatic assumption, (iv) identification and enumeration of unique microstates, (v) calculation of internal energy and entropy, (vi) theoretical model, (vii) details of molecular dynamics simulations, (viii) influence of pinned particle on the vibrational spectrum of crystallites, (ix) supplemental figures, and (x) captions for supplemental movies.

[23] J. C. Crocker and D. G. Grier, Methods of digital video microscopy for colloidal studies, J. Colloid Interface Sci. **179**, 298 (1996).

[24] W. Stöber, A. Fink, and E. Bohn, Controlled growth of monodisperse silica spheres in the micron size range, J. Colloid Interface Sci. **26**, 62 (1968).

[25] L. Zhang, M. D'Acunzi, M. Kappl, G. K. Auernhammer, D. Vollmer, C. M. van Kats, and A. van Blaaderen, Hollow silica spheres: Synthesis and mechanical properties, Langmuir **25**, 2711 (2009).

[26] R. Ganapathy, M. R. Buckley, S. J. Gerbode, and I. Cohen, Direct measurements of island growth and step-edge barriers in colloidal epitaxy, Science **327**, 445 (2010).

[27] R. W. Perry, M. C. Holmes-Cerfon, M. P. Brenner, and V. N. Manoharan, Two-dimensional clusters of colloidal spheres: Ground states, excited states, and structural rearrangements, Phys. Rev. Lett. **114**, 228301 (2015).

[28] A. Jüttner and P. Madarasi, Vf2++—an improved subgraph isomorphism algorithm, Discrete Appl. Math. **242**, 69 (2018).

[29] L. P. Cordella, P. Foggia, C. Sansone, and M. Vento, An improved algorithm for matching large graphs, in *3rd IAPR-TC15 Workshop on Graph-based Representations in Pattern Recognition* (Citeseer, 2001), p. 149.

[30] A. A. Hagberg, D. A. Schult, and P. J. Swart, Exploring network structure, dynamics, and function using networkX, in *Proceedings of the 7th Python in Science Conference (SciPy2008)*, edited by G. Varoquaux, T. Vaught, and J. Millman (Pasadena, CA, USA, 2008), p. 11.

[31] W. Feller, *An Introduction to Probability Theory and its Applications, Volume 1* (John Wiley & Sons, 1968).

[32] R. Livi and P. Politi, *Nonequilibrium Statistical Physics: A Modern Perspective* (Cambridge University Press, Cambridge, 2017).

[33] J. W. Essam, Percolation theory, Rep. Prog. Phys. **43**, 833 (1980).

[34] D. Stauffer and A. Aharony, *Introduction to Percolation Theory* (Taylor & Francis, London, 2018).

[35] M. F. Sykes and M. Glen, Percolation processes in two dimensions. I. low-density series expansions, J. Phys. A: Math. Gen. **9**, 87 (1976).

[36] J. R. Savage, D. W. Blair, A. J. Levine, R. A. Guyer, and A. D. Dinsmore, Imaging the sublimation dynamics of colloidal crystallites, Science **314**, 795 (2006).

[37] S. F. Swallen, K. L. Kearns, M. K. Mapes, Y. S. Kim, R. J. McMahon, M. D. Ediger, T. Wu, L. Yu, and S. Satija, Organic glasses with exceptional thermodynamic and kinetic stability, Science **315**, 353 (2007).

[38] L. Zhu, C. W. Brian, S. F. Swallen, P. T. Straus, M. D. Ediger, and L. Yu, Surface self-diffusion of an organic glass, Phys. Rev. Lett. **106**, 256103 (2011).

[39] A. P. Thompson, H. M. Aktulga, R. Berger, D. S. Bolintineanu, W. M. Brown, P. S. Crozier, P. J. in 't Veld, A. Kohlmeyer, S. G. Moore, T. D. Nguyen, R. Shan, M. J. Stevens, J. Tranchida, C. Trott, and S. J. Plimpton, LAMMPS - A flexible simulation tool for particle-based materials modeling at the atomic, meso, and continuum scales, Comput. Phys. Commun. **271**, 108171 (2022).

[40] K. Chen, W. G. Ellenbroek, Z. Zhang, D. T. N. Chen, P. J. Yunker, S. Henkes, C. Brito, O. Dauchot, W. Van Saarloos, A. J. Liu, and A. G. Yodh, Low-frequency vibrations of soft colloidal glasses, Phys. Rev. Lett. **105**, 025501 (2010).

[41] J. Melio, S. E. Henkes, and D. J. Kraft, Soft and stiff normal modes in floppy colloidal square lattices, Phys. Rev. Lett. **132**, 078202 (2024).

[42] A. C. Arsenault, D. P. Puzzo, I. Manners, and G. A. Ozin, Photonic-crystal full-colour displays, Nat. Photonics **1**, 468 (2007).

[43] A. Courty, A. Mermet, P. Albouy, E. Duval, and M. Pileni, Vibrational coherence of self-organized silver nanocrystals in fcc supra-crystals, Nat. Mater. **4**, 395 (2005).